Analyst

PAPER

View Article Online
View Journal | View Issue

Cite this: *Analyst*, 2026, **151**, 1786

Selective electrochemical discrimination of 3′ isomiRs differing by two nucleotides

Julio Ojeda,[a] Nicholas Bruno,[a] Karen Cover,[b] Wen Cai Zhang[b] and Karin Chumbimuni-Torres *[a]

Received 7th December 2025,
Accepted 25th January 2026

DOI: 10.1039/d5an01292a

rsc.li/analyst

MicroRNAs and isomiRs are promising biomarkers for the detection of diseases such as cancers, but distinguishing the highly similar microRNA sequences between these remains challenging. We report a five-strand four-way junction (5S-4WJ) electrochemical biosensor that combines universal reporter strands with target-specific probes for a modular, low-cost design. The system discriminates miR-146b from its isomiR (R + 2, +2 nt at 3′ end) by tuning the probe length, introducing mismatches, and controlling the hybridization kinetics. This strategy yields sevenfold higher sensitivity for R + 2 while maintaining specificity at 10–50 nM. Compared to existing electrochemical biosensors, which struggle to or do not test targets with extra nts at either 5′ or 3′, the 5S-4WJ sensor enables precise isomiR detection, advancing nucleic acid diagnostics.

Introduction

Ribonucleic acid (RNA), one of the three fundamental macromolecules alongside DNA and proteins, is distributed in various classes such as messenger RNA (mRNAs), transfer RNA, and many others.[1] One type of RNA is called non-coding RNAs (ncRNAs), which do not code for protein translation but work as modulators of gene expression at a transcriptional or post-transcriptional level.[1–3] Among the ncRNAs, microRNAs (miRNAs), which are approximately 22-nucleotide-long RNA sequences, regulate gene expression post-transcriptionally by binding to target mRNAs, resulting in inhibition of their translation. They have recently shown correlation with various human cancers.[1,4]

The common techniques for detecting miRNAs include northern blotting,[5,6] real-time quantitative polymerase chain reaction (qRT-PCR),[7,8] next generation sequencing (NGS), and microarrays, among others.[9] While these methods are powerful, they are laborious and expensive, and require trained personnel and centralized diagnostic laboratories to carry out the analysis.[10] For example, northern blotting necessitates radioactive labels, takes at least two days to evaluate miRNA levels, and exhibits lower sensitivity than other methods. qRT-PCR is the most practical method for miRNA detection; however, using locked nucleic acids, molecular beacons, TaqMan probes, or ribonucleotide-modified DNA probes makes qRT-PCR costly and complex.[7] Furthermore, qRT-PCR requires successful cDNA synthesis, which is initiated by priming miRNAs with a short adaptor strand.[11] Failure to complement the primers with miRNAs can result in false negatives.[3] NGS could be used for rapid evaluation of absolute miRNA levels; however, it is costly and less accurate due to the introduction of errors in several steps.[9]

Another challenge in miRNA detection is that for a single miRNA there is a multitude of mature miRNA variants, termed isomiRs, classified into three categories: 5′, 3′, and polymorphic (internal), depending on the sites of variations and modification types of nucleotides. For example, an isomiR could have either fewer nucleotides (Trimmed) or extra nucleotides (tailed or templated) at the 5′ or 3′.[3,4,12] The most common type of isomiR is the 3′ isomiRs, and these result from posttranscriptional trimming or from sequence tailing modifications.[13] Although these do not have a direct effect on target binding, they do have an effect on the specificity and stability of the mRNA–miRNA interactions.[14–16] Studies continue to show that the function of an isomiR is directly related to the variations in its sequence,[17] which is why the expression of isomiRs fluctuates between normal tissues and in cancers. Some cancers are reported to have isomiRs involved in chronic inflammatory diseases such as giant cell arteritis (GCA),[18] colorectal cancer,[14] lung cancer,[19] and other types of cancers.[20] Sequence variability among isomiRs influences not only their stability but also their target specificity, highlighting the need for precise isomiR detection. Even subtle mutations or nucleotide variations in miRNAs can provide critical insights into the molecular processes underlying the transformation of normal tissues into cancerous ones.[14] For all these reasons, although

[a]*University of Central Florida. Chemistry Department, Orlando, FL 32816, USA. E-mail: Karin.chumbimunitorres@ucf.edu*
[b]*University of Central Florida. Burnett School of Biomedical Sciences, College of Medicine, Orlando, FL 32827, USA*

the detection of microRNAs and their isomiRs allows promising novel approaches for early diagnosis of cancers and disease progression, there are still challenges in their detection that need to be addressed.

One approach that could address this challenge is electrochemical nucleic acid sensing. Recent advances in this field have achieved impressive sensitivity through homogeneous detection schemes, signal amplification strategies,[21] and electrode material engineering to enhance electrochemical signal transduction and stability.[22] Despite these advances, existing approaches primarily emphasize sensitivity or material performance and do not address the challenge of discriminating subtle terminal sequence variations, especially in sequences containing a few additional nucleotides at the 5′ or 3′, as in the case of isomiRs. For that reason, in this study, we have developed a modular electrochemical biosensor (e-biosensor) for the specific detection of isomiR-146b-5p (R + 2) while differentiating from its most predominant (canonical) counterpart (R), which possesses only two fewer nucleotides (a GT) at the 3′ end.

The e-biosensor design consists of two universal strands (USL and UMeB) and two target-specific strands (m and f). When the isomiR target is present, these strands assemble into a unique structure called the five-strand four-way junction (5S-4WJ, see Fig. 1). This approach optimizes the costliest elements, particularly the USL strand and UMeB redox marker, making it a feasible platform to detect multiple targets.

Experimental

Material and reagents

Trizma hydrochloride (Tris–HCl), magnesium chloride ($MgCl_2$), tris(2-carboxyethyl phosphine hydrochloride) (TCEP), 2-mercaptoethanol (MCE), 6-mercaptohexanol (MCH), 8-mercapto 1-octanol (MCO), 1-hexanethiol (HTx), and 1,6-hexanedithiol (HxDiT) were purchased from Sigma Aldrich (St Louis, USA). E-biosensor strands (m-strand, f-strand, and universal methylene blue (UMeB) strand), synthetic target fragments, a 20/100 nt ssDNA ladder, and IDTE buffer were obtained from Integrated DNA Technologies (Coralville, USA). The universal stem-loop (USL) was purchased from Biosearch Technologies, Inc. (Petaluma, USA). All oligonucleotide sequences used are shown in Table S1. Sulfuric acid 98% (H_2SO_4), potassium ferrocyanide ($K_4[Fe(CN)_6]3H_2O$), potassium ferricyanide ($K_3[Fe(CN)_6]$), sodium hydroxide (NaOH), sodium chloride (NaCl), and an ultra-low range DNA ladder were purchased from Fisher Scientific (Pittsburgh, USA). Gold disc electrodes (GDEs) were purchased from CH Instruments (Austin, USA). The alumina slurry (0.3 and 0.05 μm) was obtained from Buehler (Lake Bluff, USA). All aqueous solutions were prepared with deionized water (18.2 MΩ cm) using a Siemens PURELAB Ultra system (Lowell, USA). Immobilization buffer (IB) was prepared as follows: 50 mM Tris–HCl and 250 mM NaCl. The hybridization buffer (HB) was prepared using 50 mM Tris–HCl, 100 mM NaCl, and 50 mM $MgCl_2$. The pH of both buffers was adjusted to pH 7.40 using a 1.0 M NaOH solution.

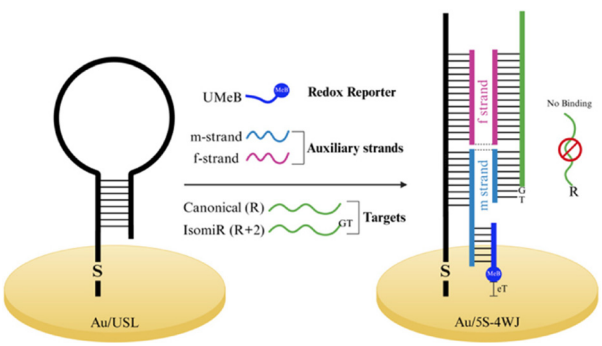

Fig. 1 Schematic representation of the 5S-4WJ formation.

Electrochemical measurement

Square-wave voltammetry (SWV) was performed using a CHI660D Electrochemical Workstation. A three-electrode system was used where the modified GDE, a platinum wire, and Ag/AgCl (1 M KCl) were used as working, counter, and reference electrodes, respectively. SWV was performed in HB from 0.0 to −0.5 V, at a frequency of 100 Hz, an amplitude of 70 mV, and a step potential of 3 mV. Nitrogen was bubbled into the HB solution of the electrochemical cell for 5 minutes to remove dissolved oxygen before measurements were taken. Current density was calculated by subtracting the measurement after 5S-4WJ formation and after immobilization with MCH. Measurements were performed in triplicate at 25 °C.

E-Biosensor preparation

The GDEs were initially cleaned *via* immersion in piranha solution (1 : 3 ratio of 30% H_2O_2 and H_2SO_4; caution – the piranha solution releases heat and should be handled with care) for 10 minutes. Next, the electrodes were manually polished using a microcloth and alumina slurry (0.3 μm then 0.05 μm) and sonicated in ethanol and deionized water to remove any residual alumina from the electrode surface, for 2 minutes each. Lastly, the GDEs were electrochemically polished *via* cyclic voltammetry (CV) from 1.6 to −0.1 V at a scan rate of 100 mV s^{-1} in 0.5 M H_2SO_4. The electrochemically active area of each GDE was calculated using the reduction gold peak from CV.[23] On average, the GDE electrodes had an area of 0.031 ± 0.004 cm^2.

To prepare the USL for immobilization, the disulfide bond was reduced by adding 25 μL of 1.0 mM TCEP in IB to 10 μL of 1.0 μM USL in IDTE buffer. This solution was then shaken for 1 hour at 25 °C. After shaking, the USL solution was further diluted using IB to a final concentration of 0.1 μM. 15 μL of the USL solution was then drop-cast onto the surface of each GDE and incubated for 30 minutes. The GDE-USL electrodes were then rinsed with IB and dried with nitrogen, and then drop-cast with 15 μL of 2 mM MCH in IB and allowed to incubate for 30 minutes.

E-Biosensor characterization

A solution containing 0.025 μM UMeB, 0.010 μM m strand, 0.050 μM f strand, and either R or R + 2 target at different concentrations was prepared in HB, as optimized in a previous work.[24] 15 μL of this solution was then drop cast onto the GDE-USL/MCH surface and incubated for several minutes. SWV was used to obtain signal measurements, as described above. The signal, expressed as the current density (j_p), was measured for three electrodes, after 5S-4WJ formation, and the baseline signal was subtracted. These triplicate values were then averaged for each concentration. The calibration curves for both targets (R and R + 2) were constructed ranging from 1 to 50 nM.

Results and discussion

The 5S-4WJ system is a multicomponent hybridization probe system composed of five DNA strands (Table S1): two universal strands (USL and UMeB), two target-specific strands (m and f), and one target strand (Fig. 1). The universal stem-loop (USL) strand is covalently immobilized on the gold electrode surface *via* a thiol bond. The m and f strands each contain two hybridization arms, one complementary to the USL and the other complementary to the target, allowing the formation of a four-way junction (4WJ) structure in the presence of the target. To enable electrochemical readout, a fifth strand is incorporated: the universal methylene blue (UMeB) strand, which carries a methylene blue redox label and hybridizes with a complementary region in the m strand. This additional reporter strand converts the 4WJ into the five-strand configuration, termed 5S-4WJ. The m strand also governs selectivity, as its short arm (8–12 nt) ensures that the 4WJ assembly occurs only when both the f and USL strands are bound to a fully complementary target. Meanwhile, the f strand facilitates target unfolding through its longer binding arm (12–22 nt), which promotes efficient hybridization.[25]

To confirm the formation of the 4WJ, the corresponding strands were diluted in HB and analyzed using native polyacrylamide gel electrophoresis. As shown in Fig. S1, a distinct band at approximately 114 nt was observed in the presence of USL, m, f, and R + 2 strands (excluding UMeB). In contrast, in the absence of the target, no 4WJ band was detected, and only individual strand bands were present. An additional band appeared near 70 nt, also visible in the USL-only sample, likely corresponding to a USL–USL dimer (each USL = 34 nt). These results confirm that 4WJ assembly occurs exclusively in the presence of the target.

A key structural component of the 5S-4WJ sensor is the mercaptoalkane self-assembled monolayer (SAM) co-immobilized with the USL. The presence and composition of the SAM significantly affect the biosensor stability and electrochemical performance.[26,27] As shown in Fig. S2, various SAM-forming molecules were evaluated for their influence on signal stability. In the absence of a SAM (black trace, Fig. S2), the signal rapidly decayed after the first scan. This decay likely arises from transient, weak interactions between DNA nucleotides and the gold surface,[28] which temporarily bring the methylene blue (MeB) moiety closer to the electrode. Once this weak interaction is disrupted after the initial scan, the signal decreases sharply.

In contrast, all SAM-modified electrodes exhibited more stable and reproducible responses, with HxDiT, MCH, HxT, and MCO producing the most consistent results. MCE, however, showed signal decay over time (Fig. S2, inset), due to incomplete surface coverage arising from its shorter, more polar chain, which limits its diffusion and adsorption from the aqueous buffer.[29,30]

Similar behaviour was observed in the absence of a target (Fig. S3). Without a SAM, the signal decayed rapidly, whereas electrodes modified with HxDiT, MCH, HxT, or MCO retained stable responses. Notably, HxDiT and HxT exhibited an additional band between −0.1 and −0.3 V, suggesting that despite improved stability, their higher background current makes them less suitable candidates.

To further examine the SAM-modified electrodes, electrochemical impedance spectroscopy (EIS) data for all SAM compositions are shown in Fig. S4A. The equivalent circuit used for fitting (Fig. S4B) includes the solution resistance (R_{sol}), double-layer capacitance (C), charge-transfer resistance (R_{ct}), and Warburg impedance (W). Among the tested SAMs, HxT exhibited the highest R_{ct}, likely due to its lower polarity, which hinders the access of water-solvated redox species such as $K_4[Fe(CN)_6]\cdot 3H_2O$ and $K_3[Fe(CN)_6]$. Among alkane–alcohol SAMs (MCE, MCH, and MCO), MCO displayed the largest R_{ct}, consistent with its longer carbon chain, as alkane chains of ≥11 carbons are known to fully passivate gold surfaces.[31] The HxDiT-modified electrode also exhibited high R_{ct} and a stronger SWV response; however, it showed a higher background current, most evident in Fig. S3 within the −0.1 to −0.3 V region. These observations are consistent with the widespread use of MCH as an optimal SAM agent in DNA-based electrochemical biosensors.[28]

With the SAM composition optimized for stable electrochemical performance, we next evaluated the biosensor's ability to discriminate between closely related nucleic acid sequences. The ability to discriminate single-nucleotide substitutions is a critical feature of electrochemical biosensors, and such selectivity tests are commonly included as part of their validation.

Typically, these assays involve introducing a single-base mismatch (MM) within the target sequence, often at the center, and comparing the signal to that of a fully matched counterpart.[32–34] However, to the best of our knowledge, no prior studies have examined biosensor performance against targets containing one or more additional nucleotides at the 5′ or 3′ termini, a distinction particularly relevant for differentiating isomiRs.

In this work, selectivity is defined as the ability of the biosensor to preferentially detect the target isomiR (R + 2) relative to the closely related sequence (R). Selectivity is assessed by comparing the corresponding current density responses.

Building on our previous work,[35,36] the m and f strands were designed to fully pair with a specific region of the RNA target. Within this framework, the 5S-4WJ architecture demonstrates strong discrimination of DNA and RNA sequences bearing a single internal mismatch within the m-strand arm. Nevertheless, in the case of the R and R + 2 targets, differing only by two additional nucleotides at the 3′ end, complete pairing of both m and f strands could lead to false-positive hybridization. Indeed, as shown in Fig. 2A, the configuration employing a long f strand (14 nt) and the m strand (8 nt) hybridized with both R and R + 2 targets across various hybridization times. Although the electrochemical responses towards R + 2 was higher than R, the design lacked true sequence specificity.

To improve selectivity toward the R + 2 target, a shortened f strand (12 nt, f short) was evaluated (Fig. 2D). The reduced binding arm was expected to hinder 5S-4WJ formation with mismatched targets. However, as shown in Fig. 2C, the R target continued to produce a measurable signal, indicating residual cross-reactivity.

To further enhance probe discrimination, the m strand was modified. Relative to the R target, the m strand binds two additional nucleotides (GT) at the 3′ end of R + 2. Yet, because these bases are terminal, their contribution to hybridization stability was minimal. Therefore, a deliberate single-nucleotide mismatch was introduced at various positions along the m strand (positions 1–8; Fig. 2F). The Gibbs free energy (ΔG°) for 5S-4WJ formation with both R and R + 2 targets was estimated using NUPACK.[37] As shown in Fig. 3, despite the introduced mismatches, hybridization with both targets remained thermodynamically favorable (ΔG° = −71.4 to −77.8 kcal mol^{-1}). This implies that thermodynamically, both R and R + 2 have the potential to hybridize and form the 5S-4WJ sensor. To choose a mismatch position for further testing, the difference in ΔG° between both configurations was calculated. The configuration with the largest predicted energy difference between R and R + 2 was that with the mismatch at position 5 (difference of −2.77 kcal mol^{-1}). Despite this being close in energy to a mismatch located at positions 6–8 (−2.76 kcal mol^{-1}), position 5 was selected for experimental validation as proof of concept.

The modified m strand (m_mm; Table S1) contained a C → A substitution at position 5 (Fig. 2F). Following this adjustment, both targets still generated detectable signals; however, the R + 2 target consistently produced higher current responses at all hybridization times, while the R target's signal approached background levels, particularly at 5 min of hybridization (Fig. 4B).

The e-biosensor was calibrated using both R and R + 2 targets (Fig. 4). After 60 minutes of hybridization, both targets exhibited linear responses, with coefficients of determination (R^2) of 0.999 for R + 2 and 0.907 for R. The sensor displayed a sensitivity toward R + 2 approximately sevenfold higher than that for R.

Despite their minimal sequence differences, both targets can thermodynamically hybridize (Fig. 3). However, kinetically,

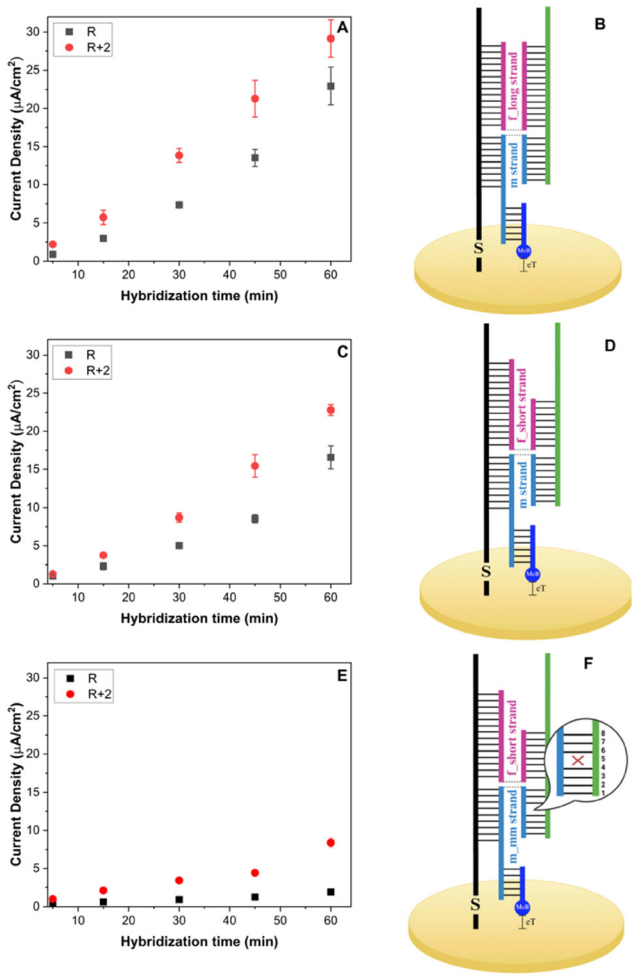

Fig. 2 Response of the e-biosensor toward 30 nM R + 2 or R target at different hybridization times (5, 15, 30, 45 and 60 minutes) on a GDE for (A) f long, m strand, (C) f short, m strand and (E) f short and m_mm. (B, D and F) Respective representation of the 5S-4WJ complex structure.

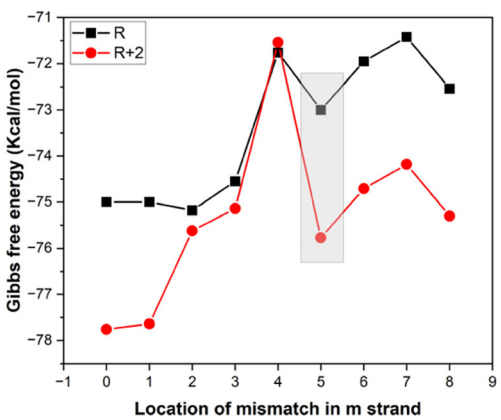

Fig. 3 Gibbs free energy of 5S-4WJ complex formation for R and R + 2 target at different modifications on the m strand binding arm.

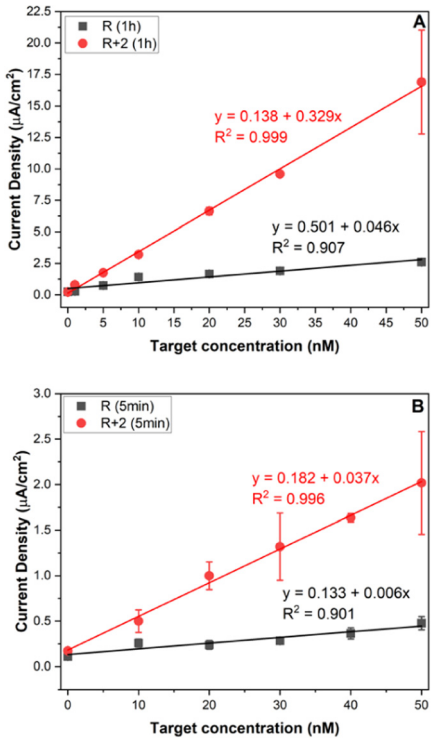

Fig. 4 Response of the e-biosensor toward (A) blank, 1, 5, 10, 20, 30, and 50 nM R + 2 or R target at 60 minutes hybridization time, and (B) blank, 10, 20, 30, 40 and 50 nM R + 2 or R target at 5 minutes hybridization time.

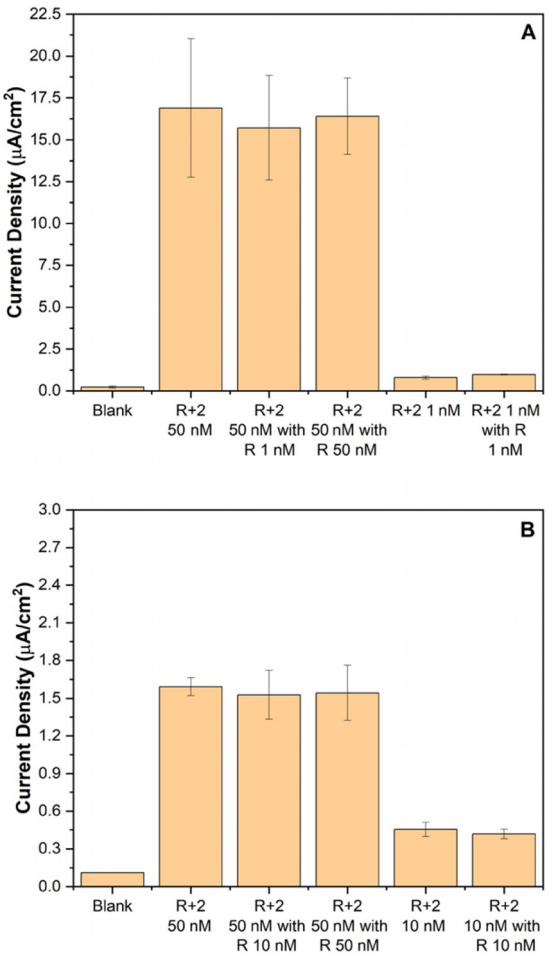

Fig. 5 Selectivity test of R + 2 in the presence of R between 10 and 50 nM at (A) 1 h hybridization time, and (B) 5 minutes hybridization time.

the 4WJ sensor exhibits a distinctive phenomenon known as kinetic inversion, as described by Stancescu *et al.*[38] In this regime, the fully matched target (R + 2), containing two additional complementary bases, stabilizes more rapidly than the mismatched R sequence. This behavior contrasts with that of linear DNA probes, where mismatched duplexes typically form faster than their fully complementary counterparts.[39,40]

Reducing hybridization time thus offers a practical route to enhance selectivity. As shown in Fig. 4B, at a 5 minute hybridization period, the R + 2 target maintained a strong linear response (R^2 = 0.996), whereas the R target exhibited a markedly lower signal, approaching that of the blank. This condition proved optimal for discriminating R + 2 even in the presence of R.

To further assess selectivity, mixtures of R and R + 2 targets at varying concentrations were hybridized with the UMeB, m_mm, and f_short strands for 1 hour and 5 minutes, respectively. After 1 hour (Fig. 5A), specificity was achieved only when the R + 2 concentration was 50 nM *vs.* 1–50 nM for R. On the other hand, when R was present at higher concentrations than R + 2 (50 nM R *vs.* 1 nM R + 2), the electrochemical response indicated the presence of both targets, producing a composite signal greater than that generated by 1 nM R + 2 alone.

At the shorter 5 minute hybridization time, the *t*-test analysis revealed that adding 10–50 nM of R to the mixture did not significantly alter the signal produced by R + 2. This indicates that, within this concentration range, the response of the e-biosensor is dominated by R + 2 binding and remains unaffected by the presence of R. These findings underscore the potential of the 5S-4WJ platform to selectively discriminate the canonical R target from the isomiR R + 2. Collectively, the results highlight an intrinsic trade-off between achieving higher current amplitudes with fully matched sequences and maximizing selectivity through shorter binding arms or deliberate mismatches.

A literature review was conducted to identify technologies capable of detecting extra nucleotides at the 5′ or 3′ ends of nucleic acids; however, no studies addressing this problem were found. As a point of comparison, we examined electrochemical biosensors reported to discriminate single-base mismatches located near these terminal regions (Table 1). Notably, no e-biosensor was able to fully differentiate sequences with variations at the 5′ or 3′ ends. To the best of our knowledge, no electrochemical biosensor has been demonstrated to distinguish mismatches, let alone additional nucleotides at either terminus, an important yet unexplored need for accurate isomiR detection.

Table 1 Comparison with e-biosensors found in the literature

Design	Technique	Location of the mismatch	LOD	Ref.
DNA pseudoknot-based e-sensor	Alternating-current voltammetry	1MM at the 5′ end of the sequence, with a signal value of 33% of the perfect match signal	Not assessed	41
Biotinylated strand with enzymatic generation of redox dye	Square wave voltammetry	1MM at the 3′ end of the sequence, with a signal value of around 50% of the perfect match signal	5–70 pM	42
Ruthenium complex able to intercalate in double stranded DNA	Differential pulse voltammetry	1MM at 4 base pairs distance from the 3′ and 5′ ends, with a signal value of 10% of the perfect match signal	92 ± 0.4 pmol	43
Biotinylated detection probe with a capture DNA probe	Linear sweep voltammetry	1MM at 4 nucleotides from 3′, with a signal value of approximately 10% of the perfect match signal	100 aM	33
Sensor based on catalytic hairpin assembly	Differential pulse voltammetry	1MM at 1 nt from 3′, with a signal value of approximately 17% of the perfect match signal	0.6 pM	44

Reported limits of detection (LODs) for electrochemical nucleic acid biosensors span a broad range, from tens of picomolar (5–70 pM) to sub-picomolar and even attomolar levels when amplification strategies are employed. While these low LODs have been reported, these studies primarily demonstrate sequence recognition capabilities rather than discrimination of terminal nucleotide variations. In contrast, the 5S-4WJ biosensor operates in the low-nanomolar regime, reflecting a design trade-off that emphasizes selective differentiation of terminal isomiR variants over achieving the lowest possible detection limit. Further work will focus on improving the LOD of this platform while preserving its ability to resolve subtle terminal sequence differences, which remain essential for accurate isomiR profiling and biological interpretation.

Conclusions

MicroRNAs remain essential biomarkers for numerous diseases, and precise detection of specific isomiRs is crucial for advancing diagnostic accuracy. In this work, the 5S-4WJ electrochemical biosensor successfully detected isomiR-146b and specifically differentiated it from its canonical miRNA, despite only a two-nucleotide difference at 3′, within a concentration range of 10–50 nM.

Author contributions

K. C. T., J. O. conceived and planned the work. J. O., N. B., K. C. conducted experiments and analyzed the results. W. C. Z. and K. C. T. supervised the project. J. O. wrote the initial draft of the manuscript with contributions from all authors. J. O., K. C., W. C. Z., K. C. T. edited the manuscript.

Conflicts of interest

There are no conflicts to declare.

Data availability

The data supporting this article have been included as part of the supplementary information (SI). Supplementary information: Table S1. Oligonucleotide sequences used in the 5S-4WJ-based biosensor. Fig. S1. Electrophoretic analysis of the 4WJ complex formation under native conditions. Fig. S2. Left: SWV response of the e-biosensor in the presence of 50 nM of R + 2 target under different SAM compositions. Fig. S3. Left: SWV response of the e-biosensor in the absence of target under different SAM compositions. Right: SWV voltammogram. Fig. S4. Left: Nyquist plots of the GDE/USL-SAM, and right: circuit model employed. See DOI: https://doi.org/10.1039/d5an01292a.

Acknowledgements

Funding from the National Science Foundation (2422986) and the National Institutes of Health (1RT5AI189259-01A1 and R03AI164938) is greatly appreciated. The authors also thank Thais Ortiz-Rodriguez for helping with image editing.

References

1 A. Esquela-Kerscher and F. J. Slack, Oncomirs—microRNAs with a role in cancer, *Nat. Rev. Cancer*, 2006, **6**(4), 259–269.
2 M. Labib and M. V. Berezovski, Electrochemical sensing of microRNAs: Avenues and paradigms, *Biosens. Bioelectron.*, 2015, **68**, 83–94.
3 R. Magee, A. G. Telonis, T. Cherlin, I. Rigoutsos and E. Londin, Assessment of isomiR discrimination using commercial qPCR methods, *ncRNA*, 2017, **3**(2), 18.
4 X. Bofill-De Ros, B. Luke, R. Guthridge, U. Mudunuri, M. Loss and S. Gu, Tumor IsomiR Encyclopedia (TIE): A pan-cancer database of miRNA isoforms, in *Bioinformatics*, ed. Y. Ponty, 2021 Sp 29, vol. 37(18), pp. 3023–3025.

5 C. G. Kevil, L. Walsh, F. S. Laroux, T. Kalogeris, M. B. Grisham and J. S. Alexander, An improved, rapid northern protocol, *Biochem. Biophys. Res. Commun.*, 1997, **238**(2), 277–279.
6 É. Várallyay, J. Burgyán and Z. Havelda, MicroRNA detection by northern blotting using locked nucleic acid probes, *Nat. Protoc.*, 2008, **3**(2), 190–196.
7 C. Chen, Real-time quantification of microRNAs by stem-loop RT-PCR, *Nucleic Acids Res.*, 2005, **33**(20), e179–e179.
8 T. D. Schmittgen, A high-throughput method to monitor the expression of microRNA precursors, *Nucleic Acids Res.*, 2004, **32**(4), 43e–443.
9 R. M. Graybill and R. C. Bailey, Emerging biosensing approaches for microRNA analysis, *Anal. Chem.*, 2016, **88**(1), 431–450.
10 X. Zhu, Y. Shen, J. Cao, L. Yin, F. Ban, Y. Shu, *et al.*, Detection of microRNA SNPs with ultrahigh specificity by using reduced graphene oxide-assisted rolling circle amplification, *Chem. Commun.*, 2015, **51**(49), 10002–10005.
11 P. Shah, S. K. Cho, P. W. Thulstrup, M. J. Bjerrum, P. H. Lee, J. H. Kang, *et al.*, MicroRNA biomarkers in neurodegenerative diseases and emerging nano-sensors technology, *J. Mol. Diagn.*, 2017, **10**(1), 18–28.
12 A. G. Telonis, R. Magee, P. Loher, I. Chervoneva, E. Londin and I. Rigoutsos, Knowledge about the presence or absence of miRNA isoforms (isomiRs) can successfully discriminate amongst 32 TCGA cancer types, *Nucleic Acids Res.*, 2017, **45**(6), 2973–2985.
13 A. Yang, X. Bofill-De Ros, T. J. Shao, M. Jiang, K. Li, P. Villanueva, *et al.*, 3′ Uridylation confers miRNAs with non-canonical target repertoires, *Mol. Cell*, 2019, **75**(3), 511–522.
14 M. A. Lausten and B. M. Boman, A review of IsomiRs in colorectal cancer, *ncRNA*, 2023, **9**(3), 34.
15 J. P. Broughton, M. T. Lovci, J. L. Huang, G. W. Yeo and A. E. Pasquinelli, Pairing beyond the seed supports microRNA targeting specificity, *Mol. Cell*, 2016, **64**(2), 320–333.
16 M. J. Moore, T. K. H. Scheel, J. M. Luna, C. Y. Park, J. J. Fak, E. Nishiuchi, *et al.*, miRNA–target chimeras reveal miRNA 3′-end pairing as a major determinant of Argonaute target specificity, *Nat. Commun.*, 2015, **6**(1), 8864.
17 S. Auddino, E. Aiello, G. E. Grieco, F. Dotta and G. Sebastiani, A three-layer perspective on miRNA regulation in β cell inflammation, *Trends Endocrinol. Metab.*, 2025, **36**(7), 623–637.
18 M. Bonacini, A. Rossi, I. Ferrigno, F. Muratore, L. Boiardi, A. Cavazza, *et al.*, miR-146a and miR-146b regulate the expression of ICAM-1 in giant cell arteritis, *J. Autoimmun.*, 2024, **144**, 103186.
19 F. M. Hsieh, S. T. Lai, M. F. Wu and C. C. Lin, Identification and elucidation of the protective isomiRs in lung cancer patient prognosis, *Front. Genet.*, 2021, **12**, 702695.
20 L. Tomasello, R. Distefano, G. Nigita and C. M. Croce, The MicroRNA family gets wider: The IsomiRs classification and role, *Front. Cell Dev. Biol.*, 2021, **9**, 668648.
21 R. Wan, Z. Zhu, X. Wang, L. Zhang, X. Huang, Y. Peng, *et al.*, Dual-signal homogeneous electrochemical system for turn-on assay of microRNA based on target-switched cyclic amplification, *J. Anal. Test.*, 2025, **9**(4), 688–693.
22 X. Huang, X. Wang, X. Wang, J. He, Z. Gao, Z. Wang, *et al.*, Template and skeleton-co-confinement pyrolysis to synthesize two-dimensional N-doped carbon nanoflakes for profiling dynamic antibiotic degradation, *J. Hazard. Mater.*, 2025, **495**, 139104.
23 S. Trasatti and O. A. Petrii, Real surface area measurements in electrochemistry, *J. Electroanal. Chem.*, 1992, **327**(1–2), 353–376.
24 M. V. Foguel, V. Zamora, J. Ojeda, M. Reed, A. Bennett, P. Calvo-Marzal, *et al.*, DNA nanotechnology for nucleic acid analysis: Sensing of nucleic acids with DNA junction-probes, *Analyst*, 2024, **149**(3), 968–974.
25 Y. V. Gerasimova and D. M. Kolpashchikov, Detection of bacterial 16S rRNA using a molecular beacon-based X sensor, *Biosens. Bioelectron.*, 2013, **41**, 386–390.
26 V. Anandan, R. Gangadharan and G. Zhang, Role of SAM chain length in enhancing the sensitivity of nanopillar modified electrodes for glucose detection, *Sensors*, 2009, **9**(3), 1295–1305.
27 R. Y. Lai, D. S. Seferos, A. J. Heeger, G. C. Bazan and K. W. Plaxco, Comparison of the signaling and stability of electrochemical DNA Sensors fabricated from 6- or 11-carbon self-assembled monolayers, *Langmuir*, 2006, **22**(25), 10796–10800.
28 T. M. Herne and M. J. Tarlov, Characterization of DNA probes immobilized on gold surfaces, *J. Am. Chem. Soc.*, 1997, **119**(38), 8916–8920.
29 Y. F. Xing, S. F. Y. Li, A. K. H. Lau and S. J. O'Shea, Electrochemical impedance spectroscopy study of mixed thiol monolayers on gold, *J. Electroanal. Chem.*, 2005, **583**(1), 124–132.
30 T. Komura, T. Yamaguchi, H. Shimatani and R. Okushio, Interfacial charge-transfer resistance at ionizable thiol monolayer-modified gold electrodes as studied by impedance spectroscopy, *Electrochim. Acta*, 2004, **49**(4), 597–606.
31 S. Campuzano, M. Pedrero, C. Montemayor, E. Fatás and J. M. Pingarrón, Characterization of alkanethiol-self-assembled monolayers-modified gold electrodes by electrochemical impedance spectroscopy, *J. Electroanal. Chem.*, 2006, **586**(1), 112–121.
32 P. Calvo-Marzal, D. Kolpashchikov and K. Chumbimuni-Torres, Nucleic acid detection using a universal electrochemical sensor for SNS differentiation, *Rev ECIPeru*, 2018, 79–86.
33 S. Hwang, E. Kim and J. Kwak, Electrochemical detection of DNA hybridization using biometallization, *Anal. Chem.*, 2005, **77**(2), 579–584.
34 T. García, M. Revenga-Parra, H. D. Abruña, F. Pariente and E. Lorenzo, Single-mismatch position-sensitive detection of DNA based on a bifunctional ruthenium complex, *Anal. Chem.*, 2008, **80**(1), 77–84.

35 A. Murray, J. Ojeda, O. El Merhebi, P. Calvo-Marzal, Y. Gerasimova and K. Chumbimuni-Torres, Cost-effective modular biosensor for SARS-CoV-2 and influenza A detection, *Biosensors*, 2023, **13**(9), 874.

36 J. Ojeda, F. Torres-Salvador, N. Bruno, H. Eastwood, Y. Gerasimova and K. Chumbimuni-Torres, Highly reproducible electrochemical biosensor for influenza A virus towards low-resource settings, *Anal. Methods*, 2024, **16**(5), 772–779.

37 J. N. Zadeh, C. D. Steenberg, J. S. Bois, B. R. Wolfe, M. B. Pierce, A. R. Khan, *et al.*, NUPACK: Analysis and design of nucleic acid systems, *J. Comput. Chem.*, 2011, **32**(1), 170–173.

38 M. Stancescu, T. A. Fedotova, J. Hooyberghs, A. Balaeff and D. M. Kolpashchikov, Nonequilibrium hybridization enables discrimination of a point mutation within 5–40 °C, *J. Am. Chem. Soc.*, 2016, **138**(41), 13465–13468.

39 S. Wang, A. E. Friedman and E. T. Kool, Origins of high sequence selectivity: A stopped-flow kinetics study of DNA/RNA hybridization by duplex- and triplex-forming oligonucleotides, *Biochemistry*, 1995, **34**(30), 9774–9784.

40 H. Dai, M. Meyer, S. Stepaniants, M. Ziman and R. Stoughton, Use of hybridization kinetics for differentiating specific from non-specific binding to oligonucleotide microarrays, *Nucleic Acids Res.*, 2002, **30**(16), e86.

41 K. J. Cash, A. J. Heeger, K. W. Plaxco and Y. Xiao, Optimization of a reusable, DNA pseudoknot-based electrochemical sensor for sequence-specific DNA detection in blood serum, *Anal. Chem.*, 2009, **81**(2), 656–661.

42 P. Abad-Valle, M. T. Fernández-Abedul and A. Costa-García, DNA single-base mismatch study with an electrochemical enzymatic genosensor, *Biosens. Bioelectron.*, 2007, **22**(8), 1642–1650.

43 T. García, M. Revenga-Parra, H. D. Abruña, F. Pariente and E. Lorenzo, Single-mismatch position-sensitive detection of DNA based on a bifunctional ruthenium complex, *Anal. Chem.*, 2008, **80**(1), 77–84.

44 Y. Zhang, Y. Yan, W. Chen, W. Cheng, S. Li, X. Ding, *et al.*, A simple electrochemical biosensor for highly sensitive and specific detection of microRNA based on mismatched catalytic hairpin assembly, *Biosens. Bioelectron.*, 2015, **68**, 343–349.